Analysis of Secondary Particles Resulting from High-Energy Nuclear Bombardment*

ROBERT W. DEUTSCH†
Department of Physics, Radiation Laboratory, University of California, Berkeley, California
(Received October 27, 1954)

Experimental studies have been made of the low-energy yields of secondary particles resulting from high-energy bombardment. For this purpose, thin foils of Be, Al, Ni, Ag, Au, and U have been bombarded by an internal beam of 375-Mev alphas, 332-Mev protons, and 187-Mev deuterons. Secondary particles emerging from the disintegration of the nucleus at 0° to the incident beam direction are magnetically analyzed and detected in nuclear emulsions located beneath the median plane of the 184-inch cyclotron. There are three specific positions for these emulsions corresponding to energies of the secondary protons and of alpha particles of approximately 6, 10, and 20 Mev. This apparatus was modified to make a special study of the secondary alpha and proton yields by including two extra plates so that 10 energy points could be taken in the range from approximately 5 to 22 Mev. The angular distribution of secondary particles has also been measured for 240-Mev alpha bombardment of Be, Al, Ni, and Ag. Here, secondary particles emitted at 0°, 45°, and 135° are detected in nuclear emulsions at positions for which the secondary proton and alpha energy is approximately 6 Mev. A secondary particle is identified by measurement of its radius of curvature upon entering the emulsion and its range and specific ionization in the emulsion. A considerable yield of hydrogen and helium isotopes as well as of particles of higher atomic number is found. The relative yields of the secondary protons and alpha particles for each element and for each bombardment are shown as a function of energy. The results, while found to be consistent with the predictions of an evaporation model, also indicate that a large percentage of secondary protons and alphas are directly knocked out of the nucleus.

INTRODUCTION

THE interaction of high-energy nucleons with nuclei is usually described qualitatively by means of a two-step process. In the first step, the incident nucleon interacts directly with a few nucleons in a nucleus. If such collisions are inelastic, mesons may be produced or if the collisions are elastic or quasi-elastic, large amounts of energy will be transferred to the nucleons and some of these will immediately ($\sim 10^{-22}$ sec) leave the nucleus. The remaining nucleons will interact quite strongly so that in a very short time (perhaps $\sim 10^{-21}$ sec) the nucleus will be in an equilibrium state that can be characterized by a temperature. In the second step, the excited nucleus then proceeds to "boil off" particles, the latter process being described by an evaporation model. Nucleons or nucleon aggregates that leave the nucleus with energies of 30 Mev or less are generally associated with the evaporation process.

Although this two-step process is generally accepted at present, some controversy exists as to which step predominates for the production of low-energy secondary particles. The evaporation hypothesis has had considerable success in predicting the energy spectrum of the secondary particles. This theory is based on the Weisskopf thermodynamical model[1] for a nucleus of mass 100 and was first applied to analyzing very high nuclear excitation by Bagge.[2] Harding, Lattimore, and Perkins,[3] and LeCouteur[4] have refined this model in analyzing cosmic-ray events so that nuclear excitation energies as high as the total nuclear binding energy of the nucleus could be used to explain the spectrum of hydrogen and helium isotopes of less than 30-Mev energy. On the other hand, Bernardini, Booth, and Lindenbaum[5] believe that while the evaporation process may account for a major portion of the low-energy protons, for a 400-Mev primary nucleon at least 25 to 40 percent of the low-energy protons are knocked out rather than evaporated off.

The experimental information is based primarily on the direct bombardment of nuclear emulsions by high-energy particles produced by cosmic rays[3,6–12] or by artificial sources.[13] The cosmic-ray bombardments show that the "black tracks," which are composed primarily of hydrogen and helium isotopes of energies below 30 Mev, have an isotropic distribution while the "grey tracks," which are composed primarily of protons of energies in the energy interval 30 to 500 Mev, have a pronounced anisotropic distribution with a peaking in the forward direction. However, Bernardini *et al.*,[13] in their experiment, in which they bombard nuclear emulsions with protons and neutrons of 300 to 400 Mev, found that while their "sparse black" and "grey track" distribution, which they define as having energies between 30 to 400 Mev, is similar to the cosmic-ray

* This paper is based on a thesis submitted in partial fulfillment of the requirements for the Ph.D. degree. The work was performed under the auspices of the United States Atomic Energy Commission.

† Now at the Knolls Atomic Power Laboratory, Schenectady, New York.

[1] V. Weisskopf, Phys. Rev. **52**, 295 (1937).
[2] E. Bagge, Ann. Physik **33**, 389 (1938).
[3] Harding, Lattimore, and Perkins, Proc. Roy. Soc. (London) **A196**, 325 (1949).
[4] K. J. LeCouteur, Proc. Phys. Soc. (London) **A63**, 259 (1950).
[5] Bernardini, Booth, and Lindenbaum, Phys. Rev. **88**, 1017 (1952).
[6] Brown, Camerini, Fowler, Heitler, King, and Powell, Phil. Mag. **40**, 862 (1949).
[7] N. Page, Proc. Phys. Soc. (London) **A63**, 250 (1950).
[8] H. L. Bradt and N. F. Kaplon, Phys. Rev. **78**, 680 (1950).
[9] D. H. Perkins, Phil. Mag. **41**, 138 (1950).
[10] Bernardini, Cortini, and Manfredini, Phys. Rev. **79**, 952 (1950).
[11] Camerini, Fowler, Lock, and Muirhead, Phil. Mag. **41** 413 (1950).
[12] Camerini, Davies, Fowler, Franzinetti, Lock, Perkins, and Yekeutieli, Phil. Mag. **42**, 1241 (1951).
[13] Bernardini, Booth, and Lindenbaum, Phys. Rev. **85**, 826 (1952).

data the angular distribution of black tracks was not found to be isotropic but there was a 25 to 40 percent excess of protons in the forward direction. They attribute the disagreement with cosmic-ray results to the difference in energy of the primary particles. According to their model, higher energy primaries induce nucleonic cascades in which preference for the incoming direction is lost by many collisions, so that the protons with less than 30 Mev of energy may be expected to have an isotropic distribution.

In addition to the emission of individual nucleons and nuclear aggregates (2, 3, 4 nucleons), the ejection of larger fragments (Z from 3 to 10) is observed from high-energy nuclear bombardment[14–16] and cosmic-ray stars.[17–21] The emission of these larger fragments has been described by Perkins.[20] He finds that the evaporation theory predicts a frequency of fragment emission much smaller than observed. The low-energy fragments can be explained by a fission process.[22] However, high-energy fragments (energies greater than 4 Mev per nucleon) are strongly collimated with incident primary particle and cannot be explained by a fission process or by a direct knock-on by the primary particle.[21]

As informative as the analysis of nuclear disintegrations in photographic emulsions may be, it leaves much to be desired. Complications are introduced by the presence of gelatin (light nuclei) in the emulsion and, of course, events occurring in Ag or Br cannot be distinguished from each other, so that a mean mass has to be assumed. Also, the statistical error in identifying particles and their energies is large. Barkas[23,24] has shown that it is possible to identify secondary particles and measure their energies by using the 184-inch cyclotron magnet as a spectrometer. The present experiment is a continuation of this method.

II. EXPERIMENTAL ARRANGEMENT AND PROCEDURE

The entire experiment is performed beneath the circulating beam of the 184-inch cyclotron. The magnetic field of the cyclotron provides a means for analyzing the momentum of secondary particles emitted from an internal target. Nuclear track emulsions are employed to detect the secondary particles.

Two specific experimental arrangements have been constructed to utilize an existing cart, 40 in. by 20 in., which enters the cyclotron pressure chamber through an air lock. This cart can be placed in position beneath the circulating beam. One arrangement (Fig. 1) measures the relative abundances of secondary particles emitted at 0° for three different radius-of-curvature intervals. The other arrangement (Fig. 2) measures the relative abundances of secondary particles emitted at three different angles for one radius-of-curvature interval.

For both arrangements, the beam is clipped radially by a carbon block which is located on the opposite side of the cyclotron from the target. The beam is clipped at a radius two inches greater than the target radius. Vertical oscillations are also clipped by a copper block lowered into the beam so that the height of the beam at the target is largely confined to $\frac{3}{4}$ inch as determined by radioautographs of the target.

The nuclear-track plates which are used as detectors are 200μ Ilford C2 emulsions. These emulsions are of moderate sensitivity, so as to obtain some ionization discrimination and yet to be able to see higher energy protons in the emulsion.

A. Momentum Distribution at 0° (Fig. 1)

Thin ribbon targets extending parallel to the magnetic field are placed with their smaller dimension perpendicular to the beam direction. These targets are exposed at a radius of 79 inches, corresponding to bombarding energies of protons of 332 Mev, deuterons of 187 Mev, and alpha particles of 375 Mev. Secondary particles then spiral down into nuclear emulsions which are placed at three specific positions along a radial line of the cyclotron. For the area of the plates that were scanned, these positions correspond to radius-of-curvature interval of 21–24.5 cm, 29–32.5 cm, and 42–46 cm. The nuclear-track plates are placed with emulsion upward in a plane parallel to the median plane of the cyclotron. The plates are $5\frac{1}{2}$ inches below the median plane for 21–24.5 cm and 29–32.5 cm positions, and $4\frac{1}{4}$ inches for the 42-46 cm position. The plates had to be raised for the 42–46 cm position so the orbits of the secondary particles could clear the edge of the cart. Shielding, of brass and copper, is placed around the plates to protect them against stray particles from the main beam and against neutrons from the target. Channels are built in the shielding so that particles with a plane projected angle of $\pm 10°$ can enter the plates.

In order to get more data for a separate study of the energy spectra of protons and alpha particles, the apparatus was modified by the addition of two plate positions, one plate falling between the plates at 21–24.5 cm and 29–32.5 cm positions located at $5\frac{1}{2}$ inches below median plane and the other between the 29–32.5 cm and 42–46 cm positions located $4\frac{1}{4}$ inches below median plane. In order to improve the resolution and get additional data, two narrow regions were scanned on each plate. The radius-of-curvature intervals for the positions scanned were the following:

[14] S. C. Wright, Phys. Rev. **79**, 838 (1950).
[15] L. Marquez and I. Perlman, Phys. Rev. **81**, 953 (1951).
[16] R. E. Batzel and G. T. Seaborg, Phys. Rev. **82**, 607 (1951).
[17] A. Bonnetti and C. Delworth, Phil. Mag. **40**, 585 (1949).
[18] P. Hodgson and D. H. Perkins, Nature **163**, 439 (1949).
[19] S. O. C. Sorensen, Phil. Mag. **40**, 947 (1949).
[20] D. H. Perkins, Proc. Roy. Soc. (London) **A23**, 399 (1950).
[21] S. O. C. Sorensen, Phil. Mag. **42**, 188 (1951).
[22] Y. Fujimoto and Y. Yamaguchi, Progr. Theoret. Phys. (Japan) **5**, 76 (1950).
[23] W. Barkas and J. Bowker, Phys. Rev. **87**, 205 (1952).
[24] W. Barkas and H. Tyren, Phys. Rev. **89**, 1 (1953).

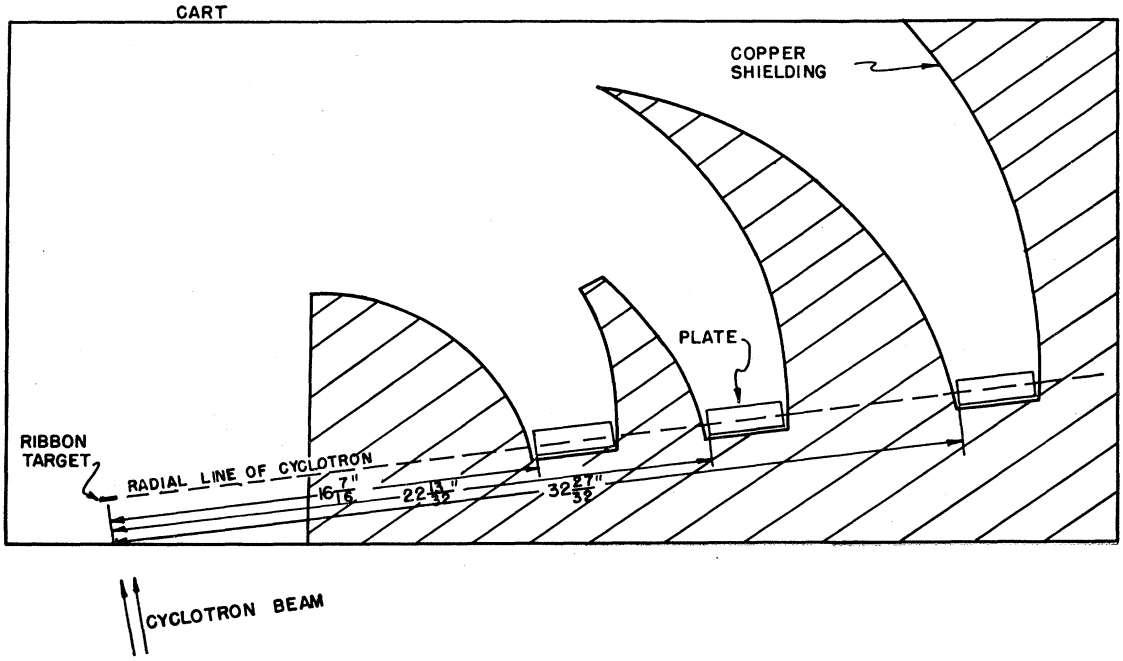

FIG. 1. Plan view of arrangement of apparatus to measure relative abundances of secondary particles emitted at 0° for three different radius-of-curvature intervals. The cart, loaded with copper shielding and with plates in the positions shown, enters the cyclotron vacuum tank through an air lock. The cart is low enough to be entirely underneath the circulating beam. The secondary particles spiral down slightly and enter the plates through the surface of the emulsion. Blocks of wolfram are placed as roofs over the plates to reduce stray light and background tracks.

Plate position	Radius-of-curvature intervals (cm):
1	21.3–22.7, 23.5–24.9
2	25.4–26.8, 27.6–29.0
3	29.4–30.9, 31.6–33.1
4	35.9–37.5, 38.2–39.8
5	42.5–44.1, 44.7–46.4

B. Angular Distribution (Fig. 2)

This apparatus detects particles which are emitted at angles of 0°, 45°, and 135° to the incident-beam direction. In order to contain the orbits of secondary particles in regions of nearly constant magnetic field, the targets are exposed at a radius of 62 inches and mounted in the previously described manner. Thus the effective target thickness for the secondary particle is $\sqrt{2}$ greater for the 45° and 135° position than for 0°. The radius-of-curvature interval for each position is 21–24.5 cm. At a 62-inch radius, the beam is only $2\frac{7}{8}$ inches above the plates. The elevation of the beam, coupled to the fact that only a limited amount of shielding could be placed around the plate, permitted only alpha bombardment as proton and deuteron bombardment blackened the plates with background tracks. The alpha energy at 62 inches is 240 Mev. The channels in the shielding permit particles with a plane projected angle of $0°\pm10°$, $45°\pm10°$, and $135°\pm10°$ to enter the plates in each position.

C. Targets

The targets are thin foils prepared by commercial methods. The amount of contamination should be <1 percent (no experimental verification was made of the purity of each element, however). Uranium is undoubtedly contaminated by the formation of an oxide which may be >1 percent. The target thickness is as follows, in mg/cm²:

Be—8.67,	Ag—12.8,
Al—1.67,	Au—11.7,
Ni—8.10,	U—23.0.

D. Microscope Measurements

The plates are scanned under $\sim$1000× magnification. The position, range, plane-projected angle, and charge of each track on a measured area of plate are recorded. Only tracks having the proper dip angle while entering the emulsion within $\pm10°$ of the mean plane projected angle for that plate are accepted. The ranges are measured by means of a calibrated reticule placed in the eyepiece of the microscope. However, some of the very long proton ranges ($\sim1800\mu$) were also measured by means of the microscope stage coordinates. The angles are measured within an accuracy of $\pm1°$ by a goniometer affixed to the eyepiece. For most positions, the charge-one secondary particles (hydrogen isotopes) can be separated by eye from the higher-charge second-

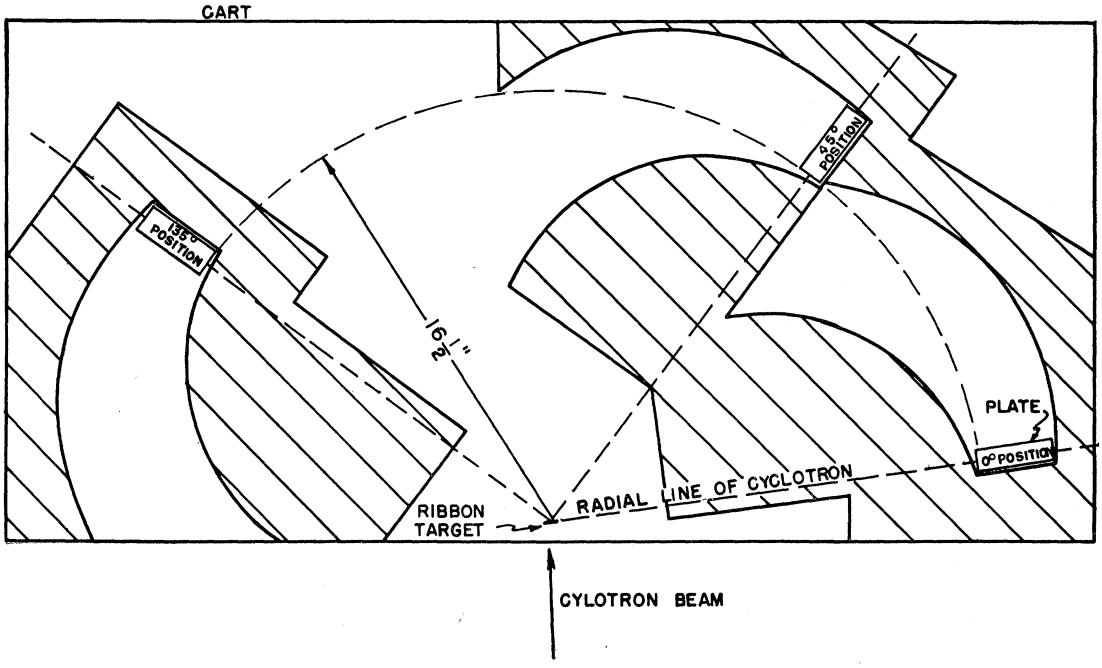

FIG. 2. Plan view of arrangement of apparatus to measure relative abundances of secondary particles emitted at 0°, 45°, and 135° for one radius-of-curvature interval. (Cart, shielding, and geometry as in Fig. 1.)

ary particles. The charge is recorded as one or greater than one. For those cases (to be discussed in the next section), where there is doubt concerning the charge, a measure of the specific ionization is made by recording the number of gaps in each track where there are no developed grains. Tracks were not recorded unless they were at least 9 microns long. This range was selected arbitrarily as a range that would not be overlooked by the observer, as well as being of sufficient length to get an accurate angle measurement.

III. METHOD OF ANALYSIS OF SECONDARY PARTICLES

A. Calculation of Range, Radius of Curvature, and Acceptable Range Interval

In order to identify the secondary particles, one makes use of a set of curves in which the range in emulsion is calculated for each isotope and plotted as a function of radius of curvature (as in Fig. 4). In such a diagram each nuclear type falls on a characteristic locus. A point is plotted on the same graph, from an experimental determination of the range and radius of curvature. The position at which the point falls on the curve identifies the particle.

The calculation of the ranges involves first finding the $H\rho$ and, consequently, the energy of each particle. An expression for the $H\rho$ of a particle moving in the median plane of the nonuniform field of the cyclotron has been previously derived.[25] This expression, in which the trajectories are described in cylindrical coordinates (r,θ,z) and which is corrected for an orbit lying slightly outside the median plane, is

$$H\rho=\sec\gamma\int_{r_1}^{r_2}H(r)rdr\Big/(r_1\cos\lambda_1-r_2\cos\lambda_2),\quad(1)$$

where the subscripts refer to any point on the orbit, $\tan\lambda=(1/r)dr/d\phi$ and γ is the angle of pitch of the spiral path. For the special case of an orbit whose initial and final trajectories intersect the same radial line (all positions in Fig. 1 and 0° position in Fig. 2), (1) reduces approximately (error <0.1 percent) to

$$H\rho=\sec\beta\sec\gamma\int_{r_1}^{r_2}H(r)rdr\Big/(r_1+r_2),\quad(2)$$

where β is the plane-projected angle measured with respect to a line perpendicular to the radial line. For cases of the 45° and 135° positions in Fig. 2, the expression is slightly more complicated. The magnetic field of the cyclotron has been measured (relative field values are accurate to $\sim$0.02 percent but the absolute value of the field could be off by as much as 0.1 percent) and $H\rho$ calculated by a numerical integration.

Table I shows the secondary particles considered and their mean energies in each plate not corrected for energy loss in the target. Carbon is the highest atomic number considered, because the range-energy curves have not been verified for higher atomic number and because the resolution becomes very poor.

[25] W. H. Barkas, Phys. Rev. 78, 90 (1950).

Knowing the energies, we find the ranges in emulsion of the hydrogen and helium isotopes by using the published data of Wilkins.[26] For the heavy secondary particles, the ranges are found by using the range-energy curves for the alpha particles and making use of an empirical expression which describes the range extension introduced by electron pickup.[27]

Figure 3 shows a diagram of an orbit traveled by a particle upon leaving the target. From simple geometrical considerations and with the assumption of a uniform magnetic field, the radius of curvature, ρ, is

$$\rho=\rho_H \sec\gamma=\frac{d}{2}\sec\beta\left(1+\frac{4h^2\cos^2\beta}{(\pi\pm2\beta)^2d^2}\right)^{\frac{1}{2}}, \qquad (3)$$

where ρ_H is the horizontal projection of ρ, γ is the angle of pitch $[\tan^{-1}(h/\pi\rho_H)]$, d is the distance from the target measured along the x axis at which a particle enters the emulsion, h is the height of the beam above the emulsion, and β is the plane projected angle (whose sign depends on the direction of the particle entering the plate). We can correct ρ by taking into account the nonuniformity of the field. That is, more exactly, $\rho=(H\rho)/\bar{H}$ where $H\rho$ is determined from (2) and $\bar{H}$ is the mean value of the magnetic field for the orbit. The values for ρ determined by the two methods differ by $<0.002\rho$.

The calculated-range-*versus*-ρ curve gives a characteristic locus for each nuclear type. However, this calculation has to be verified experimentally because there is possible variation in the stopping power of the emulsion and error in the determination of the absolute value of the magnetic field. An experimental check was made by measuring the range-energy curve for alpha particles. There was agreement to better than 1 percent for the calculated curves in all plate positions.

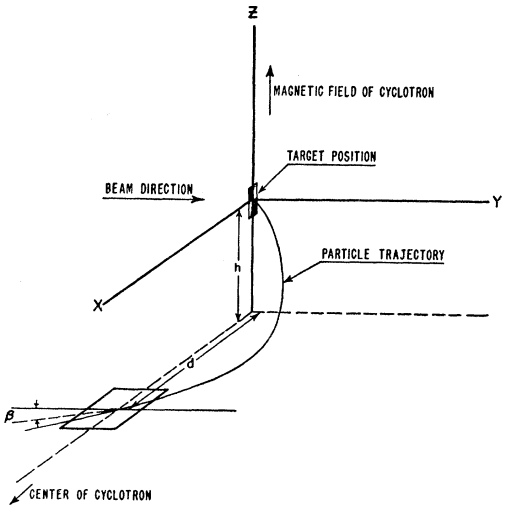

FIG. 3. Schematic diagram of the trajectory of a secondary particle emerging from target and spiraling down and entering nuclear emulsion with plane projected angle β.

In order to determine how far from a calculated locus the range of a particle may fall and still be included as belonging to that locus, the range straggle was measured for the hydrogen and helium isotopes. The standard deviation was found to be nearly constant for all ranges and to be 3 percent or less of the range. (The range straggle includes the usual Bohr straggling, the effect of the finite width of the target, and observer errors.) The acceptable band width for each locus was taken as $\pm2\frac{1}{2}$ standard deviations or $\pm7\frac{1}{2}$ percent of the range.

Protons have by far the longest range in each position and also undergo the most scattering. They could not be measured to the same accuracy as the other particles without consuming an inordinate amount of time. The band width for protons was widened to ±10 percent to allow for less accurate measurements. Protons in the 42–46 cm position, which have a range of 1800μ, frequently ($\sim$30 percent) scatter out of the plate before coming to the end of their range.

In order to determine the number of protons that come from the target, a plot is made of the protons that leave the emulsion. The protons that have too long a range to have come from the target determine the background. It is found that the background protons constitute about 30 percent of the protons leaving the plate.

TABLE I. Mean energies of secondary particles in Mev for the radius-of-curvature intervals considered. (These energies are uncorrected for energy loss in the target, although it is significant for particles of short range.)

Radius-of-curvature interval	21–24.5 cm	29–32.5 cm	42–46 cm
H^1	5.1	9.4	19.2
H^2	2.6	4.7	9.6
H^3	1.7	3.1	6.4
He^3	6.9	12.5	25.7
He^4	5.2	9.4	19.3
He^6	3.4	6.3	12.9
Li^6	7.7	14.1	29.0
Li^7	6.6	12.1	24.8
Li^8	5.8	10.6	21.7
Li^9	5.2	9.5	19.4
Be^7	11.8	21.6	44.1
Be^9	9.2	16.8	34.3
Be^{10}	8.2	15.1	30.9
B^8	16.1	29.5	60.3
B^{10}	12.9	23.6	48.3
B^{11}	11.7	21.5	43.9
B^{12}	10.8	19.7	40.3
C^{10}	18.6	34.0	69.6
C^{11}	16.9	30.9	63.3
C^{12}	15.5	28.4	58.1
C^{13}	14.3	26.2	53.6
C^{14}	13.3	24.3	49.8

[26] J. J. Wilkins, Atomic Energy Research Establishment, Harwell Report G/R 664, 1951 (unpublished).
[27] W. H. Barkas, Phys. Rev. **89**, 1019 (1953).

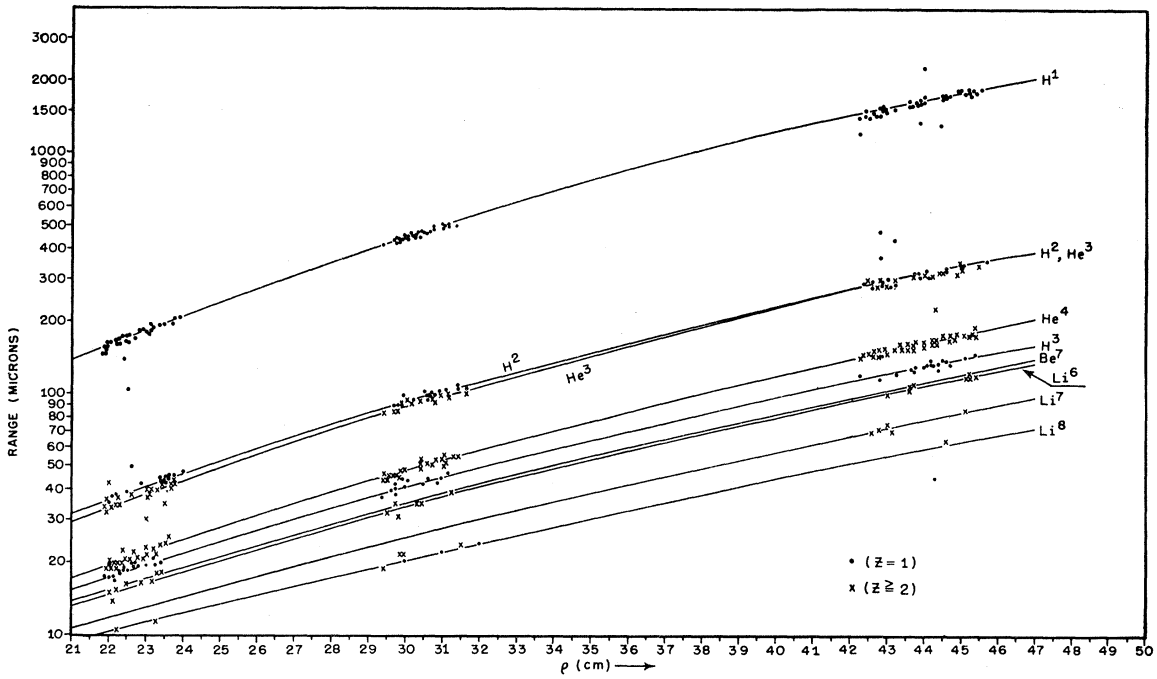

FIG. 4. Representative sample of secondary particles resulting from 375-Mev alpha bombardment of Be. The solid lines are the calculated loci for most of the isotopes considered. The charge of each particle is determined to be one or greater than one by determination of the specific ionization. Particles whose ranges are displaced more than $7\frac{1}{2}$ percent of the calculated range are regarded background.

There is some overlap of ranges for the hydrogen and helium isotopes, notably H^2 and He^3, for all positions. Identification of such tracks was made by gap count. If G is the number of gaps in a residual range R, and M is the ionic atomic weight, then $G/M=f(R/M)$, where $f(R/M)$ is the same function of (R/M) for all isotopes of an element. Curves of $f(R/M)$ prepared from tracks of all isotopes which have been identified provided means for separating completely H^2 and He^3. There is also a slight overlap between H^3 and He^4 in the 21–24.5 cm position, and it was necessary to narrow the acceptable band width to 6 percent of the range for this case, as the tracks for these particles are too dense to separate by gap count.

Only a few of the heavier particles can be identified individually. Li^8 and B^8 can always be distinguished from others by the characteristic hammer at the ends of their tracks and from each other by their ranges. Li^7 can be separated only in the 42–46 cm position. Li^6 and Be^7 together form a common locus which is separable in each position, although there is possible contamination with carbon isotopes in the 21–24.5 cm position. For these particles also, a $\pm 7\frac{1}{2}$ percent band width was taken, except for Li^6 and Be^7 in the 21–24.5 cm position, where the band width was 6 percent of the range.

Figure 4 shows the calculated loci for the secondary particles that could be identified individually, together with a representative sample of experimentally determined points for one of the bombardments using the 0° apparatus.

For the remaining secondary particles listed in Table I, there is an overlap of ranges, and separation was therefore attempted by grouping the calculated loci together wherever possible. The groups chosen are shown in the table of results. They were chosen arbitrarily and could very well overlap. The small number of these particles found does not justify going into greater detail. Only tracks which were greater than 9μ were accepted. All tracks that had a range greater than 9μ but were still too short to fall on any calculated locus were listed in the "not classified" group. For the 29–32.5 cm and the 42–46 cm positions, the members of these groups are fission fragments or members of the other groups that are not fully stripped of electrons when they leave the target. The resolution decreases in going from the 42–46 cm plate to the 21–24.5 cm plate. In the latter position, Li^6 and Be^7 were the only heavy particles that could be separated; all the rest fell so close together that it was not even possible to separate by groups, and they were all listed in the "not classified" group for this position.

B. Background

The general background is very definitely a function of the element used as target. Unfortunately, it is not possible to measure the background experimentally by removing the target. The target acts as a beam clipper

as well as a neutron source, so that conditions are not comparable when the target is absent. Since the same amount of shielding for the plates is used with each kind of bombarding particle, the general background may also be expected to be a function of the range of the bombarding particle in the shielding. The background resulting from alpha and deuteron bombardment is very much less than the background resulting from proton bombardment. Nevertheless, the background tracks, which arise principally from the scattered beam and neutrons striking the cart and shielding, are not a serious problem. The angle criteria (accepting only tracks of the proper projected and dip angles) rule out most of the background. With the exception of protons, practically all the secondary particles (~98 percent) fall within the calculated range intervals. The situation for the heavy-particle groups and "not classified" group is slightly ambiguous, as there is no range criterion to eliminate background here. However, only tracks which can be observed to have a charge of two or greater are included in this group and this type of background (charge 2 or greater) is believed to be small. Almost all the background tracks which satisfy the angle criteria and do not fall within calculated range intervals are protons, and most of these protons fall well outside the calculated range interval.

C. Solid Angle Factor and Reduction of Data

In making a comparison of the data from different plates, one must take into account the solid angle subtended by each plate. It is necessary to transform the plate coordinates (x,y,β) into the target coordinates (ρ,θ,ϕ). That is, it is necessary to transform the number of tracks found per unit area per angular interval on the plate into the number of particles per unit solid angle per unit radius-of-curvature interval leaving the target. This transformation[28] is accomplished by means of a Jacobian, J, such that:

$$\frac{\Delta N}{\Delta\rho\Delta\omega}=\frac{\Delta N}{\Delta\rho\Delta\cos\theta\Delta\phi}=J\left(\frac{x_1y_1\beta}{\rho,\theta,\phi}\right)\frac{\Delta N}{\Delta x\Delta y\Delta\beta}. \quad (4)$$

The value of the Jacobian is

$$|J|=\frac{2h}{\cos^2\theta}\sin^2\frac{h}{2\rho\cos\theta}.$$

For the special case of 180° focussing, as we have in the two experimental arrangements, the Jacobian reduces to $2h[1+(\pi\rho_H/h)^2]$, where h is the height of the beam above the plate and ρ_H is the horizontal projection of the radius of curvature. This Jacobian is needed as a weighting factor to reduce the data for

TABLE II. Relative abundances of products emitted at 0° to the incident beam direction for 375-Mev alpha bombardment. Each element has been normalized to 100 percent for the number of particles found per unit solid angle per unit radius-of-curvature interval. The actual numbers of tracks found are in parentheses and are listed below the percentages in each case.

Rad.-of-curv. interval	42–46 cm						29–32.5 cm						21–24.5 cm					
Element	Be	Al	Ni	Ag	Au	U	Be	Al	Ni	Ag	Au	U	Be	Al	Ni	Ag	Au	U
H^1	10.92 (163)	12.10 (199)	13.36 (239)	17.37 (194)	29.62 (178)	28.74 (204)	8.36 (119)	13.57 (214)	26.88 (401)	38.56 (499)	19.59 (402)	9.79 (271)	6.50 (125)	14.82 (276)	31.16 (491)	15.90 (508)	1.67 (196)	2.45 (137)
H^2	3.62 (54)	2.43 (40)	2.63 (47)	3.40 (38)	3.16 (19)	2.26 (16)	3.94 (56)	1.97 (31)	0.87 (13)	0.15 (2)	0.09 (2)	0.33 (9)	2.08 (40)	0.65 (12)	0.19 (3)	0.06 (2)	0.14 (16)	0.25 (14)
H^3	2.75 (41)	0.48 (8)	0.34 (6)	0.09 (1)	0.17 (1)	0.42 (3)	2.32 (33)	0.19 (3)	0.34 (5)	0.15 (2)	0.09 (2)	0.25 (7)	1.51 (29)	0.43 (8)		0.03 (1)	0.08 (9)	0.15 (8)
He^3	2.68 (40)	1.46 (24)	1.29 (23)	1.07 (12)	1.16 (7)	1.13 (8)	4.29 (61)	1.33 (21)	1.01 (15)	0.08 (1)	0.15 (3)	0.47 (13)	2.76 (53)	0.59 (11)	0.38 (6)	0.06 (2)	0.17 (20)	0.27 (15)
He^4	10.52 (157)	9.67 (159)	7.88 (141)	17.46 (195)	28.29 (170)	18.60 (132)	19.19 (273)	14.97 (236)	8.51 (127)	2.24 (29)	1.17 (24)	3.87 (107)	12.59 (242)	11.70 (218)	2.22 (35)	0.25 (8)	0.49 (58)	4.01 (224)
Li^6, Be^7	0.74 (11)	0.42 (7)	0.50 (9)	0.63 (7)	1.50 (9)	1.55 (11)	0.63 (9)	1.14 (18)	0.47 (7)		0.34 (7)	0.47 (13)	0.83 (16)	0.48 (9)	0.19 (3)		0.43 (5)	0.38 (21)
Li^7	0.33 (5)	0.48 (8)	0.34 (6)	0.27 (3)	0.83 (5)	0.28 (2)												
Li^8	0.07 (1)					0.14 (1)	0.28 (4)						0.16 (3)					0.02 (1)
B^8	0.07 (1)	0.06 (1)												0.05 (1)				
I	0.27 (4)	0.42 (7)	0.06 (1)	0.27 (3)	0.17 (1)		0.77 (11)	1.46 (23)	0.47 (7)	0.38 (5)	0.68 (14)	0.43 (12)						
II	0.07 (1)	0.18 (3)	0.06 (1)	0.09 (1)	0.17 (1)	0.42 (3)	0.21 (3)	1.27 (20)	0.14 (2)	0.08 (1)	0.09 (2)	0.32 (9)						
III		0.12 (2)	0.06 (1)	0.18 (2)		0.71 (5)												
Not classified	0.13 (2)	0.61 (10)	0.22 (4)	0.81 (9)	8.15 (49)	16.91 (120)	0.07 (1)	3.30 (52)	0.14 (2)	0.23 (3)	1.27 (26)	4.05 (112)	1.35 (26)	3.60 (67)	0.32 (5)	0.18 (6)	0.31 (37)	1.36 (76)
		I —He^6, Be^9, B^{10}, C^{11} II —Be^{10}, B^{11}, C^{12}, C^{13} III—He^7, Li^9, B^{12}, C^{14}						I —He^6, Li^7, Be^9, Be^{10}, B^{10}, B^{11}, C^{11}, C^{12}, C^{13} II—He^7, Li^9, B^{12}, C^{14}										

[28] W. H. Barkas. University of California Radiation Laboratory Report UCRL-2126 (unpublished).

TABLE III. Relative abundances of products emitted at 0° to the incident beam direction for 332-Mev proton bombardment. Each element has been normalized to 100 percent for the number of particles found per unit solid angle per unit radius-of-curvature interval. The actual numbers of tracks found are in parentheses and are listed below the percentages in each case.

Rad.-of-curv. interval	42–46 cm						29–32.5 cm						21–24.5 cm					
Element	Be	Al	Ni	Ag	Au	U	Be	Al	Ni	Ag	Au	U	Be	Al	Ni	Ag	Au	U
H^1	12.22 (96)	14.10 (146)	9.47 (132)	15.63 (104)	51.50 (138)	34.61 (109)	7.47 (61)	16.02 (120)	27.36 (183)	45.03 (241)	20.16 (200)	8.90 (105)	10.82 (87)	22.21 (165)	40.11 (256)	16.74 (260)	1.45 (136)	2.26 (109)
H^2	4.84 (38)	3.38 (35)	1.94 (27)	3.91 (26)	1.86 (5)	2.54 (8)	3.92 (32)	1.86 (14)	1.05 (7)			0.76 (9)	2.74 (22)	0.40 (3)		0.12 (2)	0.05 (5)	0.11 (5)
H^3	2.67 (21)	0.58 (6)	0.07 (1)	1.05 (7)		0.32 (1)	1.96 (16)	0.26 (2)		0.19 (1)	0.21 (2)	0.42 (5)	1.37 (11)	0.27 (2)		0.06 (1)	0.01 (1)	0.06 (3)
He^3	3.31 (26)	0.96 (10)	0.86 (12)	0.60 (4)	0.37 (1)	0.95 (3)	2.81 (23)	0.26 (2)	0.90 (6)	0.37 (2)		0.34 (4)	2.74 (22)	0.94 (7)	0.31 (2)		0.04 (3)	0.25 (12)
He^4	8.40 (66)	6.37 (66)	3.95 (55)	12.62 (84)	22.77 (61)	9.84 (31)	14.32 (117)	15.49 (116)	10.91 (73)	2.80 (15)	0.21 (2)	2.96 (35)	14.68 (118)	12.25 (91)	2.04 (13)	0.19 (3)	0.23 (21)	2.07 (100)
Li^6, Be^7	0.64 (5)		0.22 (3)	0.15 (1)		0.64 (2)	1.48 (12)	0.26 (2)	0.30 (2)		0.10 (1)	0.16 (2)	0.62 (5)	0.40 (3)			0.05 (5)	0.16 (8)
Li^7	0.25 (2)		0.07 (1)															
Li^8							0.24 (2)						0.25 (2)					
B^8																		
I	0.25 (2)		0.07 (1)	0.15 (1)			0.98 (8)	1.32 (10)	0.15 (1)	0.19 (1)		0.42 (5)						
II					0.37 (1)			0.53 (4)		0.19 (1)		0.09 (1)						
III																		
Not classified		0.11 (1)	0.07 (1)		0.37 (1)	24.77 (78)	0.24 (2)	0.80 (6)			0.21 (2)	7.04 (83)	0.75 (6)	1.21 (9)	0.16 (1)		0.05 (4)	0.31 (15)
	I —He^6, Be^9, B^{10}, C^{11} II —Be^{10}, B^{11}, C^{12}, C^{13} III—He^7, Li^9, B^{12}, C^{14}						I —He^6, Li^7, Be^9, Be^{10}, B^{10}, B^{11}, C^{11}, C^{12}, C^{13} II—He^7, Li^9, B^{12}, C^{14}											

TABLE IV. Relative abundances of products emitted at 0° to the incident beam direction for 187-Mev deuteron bombardment. Each element has been normalized to 100 percent for the number of particles found per unit solid angle per unit radius-of-curvature interval. The actual numbers of tracks found are in parentheses and are listed below the percentages in each case.

Rad.-of-curv. interval	42–46 cm						29–32.5 cm						21–24.5 cm					
Element	Be	Al	Ni	Ag	Au	U	Be	Al	Ni	Ag	Au	U	Be	Al	Ni	Ag	Au	U
H^1	7.65 (166)	9.49 (180)	10.48 (230)	17.36 (206)	29.26 (177)	29.63 (312)	9.83 (143)	15.56 (255)	28.40 (403)	35.76 (473)	26.99 (349)	9.76 (264)	9.96 (80)	25.51 (166)	37.58 (257)	18.29 (325)	1.87 (87)	2.08 (117)
H^2	3.87 (84)	3.11 (59)	2.23 (49)	4.80 (57)	3.80 (23)	2.56 (27)	4.74 (69)	2.01 (33)	0.99 (14)	0.45 (6)	0.23 (3)	0.37 (10)	3.11 (25)	1.23 (8)	0.29 (2)		0.04 (2)	0.27 (15)
H^3	2.90 (63)	0.68 (13)	0.41 (9)	1.09 (13)	0.33 (2)	0.57 (6)	3.65 (53)	0.49 (8)		0.07 (1)	0.15 (2)	0.21 (6)	2.99 (24)	0.77 (5)	0.14 (1)			0.11 (6)
He^3	1.52 (33)	1.26 (24)	0.50 (11)	1.09 (13)	0.99 (6)	0.67 (7)	4.47 (65)	1.28 (21)	0.63 (9)	0.52 (7)	0.15 (2)	0.41 (11)	3.24 (26)	0.31 (2)	0.14 (1)	0.06 (1)	0.02 (1)	0.11 (6)
He^4	5.63 (122)	6.32 (120)	4.15 (91)	12.88 (153)	26.12 (158)	17.28 (182)	18.78 (273)	13.54 (222)	10.01 (142)	5.60 (74)	0.77 (10)	2.21 (60)	13.33 (107)	13.37 (87)	2.63 (18)	0.17 (3)	0.34 (16)	6.81 (383)
Li^6, Be^7	0.46 (10)	0.32 (6)	0.05 (1)		0.66 (4)	0.47 (5)	0.89 (13)	0.43 (7)	0.35 (5)	0.07 (1)	0.39 (5)	0.25 (7)	0.75 (6)	0.31 (2)			0.02 (1)	0.08 (5)
Li^7	0.23 (5)	0.37 (7)	0.09 (2)	0.17 (2)	0.17 (1)	0.57 (6)												
Li^8	0.05 (1)	0.05 (1)	0.05 (1)	0.09 (1)														
B^8																		
I	0.05 (1)		0.09 (2)		0.33 (2)	0.19 (2)	0.89 (13)	0.79 (13)	0.28 (4)	0.14 (2)	0.69 (9)	0.22 (6)						
II		0.11 (2)	0.05 (1)		0.82 (5)	0.19 (2)	0.21 (3)	0.43 (7)	0.14 (2)		0.23 (3)	0.25 (7)						
III	0.09 (2)			0.17 (2)	0.50 (3)	0.19 (2)												
Not classified	0.51 (11)	0.79 (15)	0.32 (7)	1.09 (13)	4.30 (26)	15.95 (168)	0.07 (1)	0.55 (9)		0.07 (1)	0.69 (9)	8.06 (218)	0.12 (1)	0.92 (6)		0.06 (1)	0.13 (6)	0.50 (28)
	I —He^6, Be^9, B^{10}, C^{11} II —Be^{10}, B^{11}, C^{12}, C^{13} III—He^7, Li^9, B^{12}, C^{14}						I —He^6, Li^7, Be^9, Be^{10}, B^{10}, B^{11}, C^{11}, C^{12}, C^{13} II—He^7, Li^9, B^{12}, C^{14}											

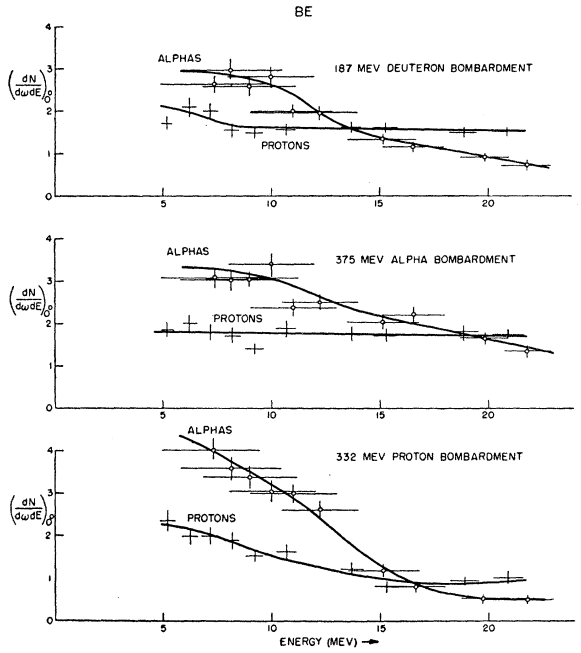

FIG. 5. Yields of secondary protons and alphas emitted at 0° to the incident beam direction as a function of their energy. The yields of protons and alphas are relative to each other and the ordinate is in arbitrary units. Smooth curves have been arbitrarily drawn through the points. The errors shown for the number of particles found are statistical standard deviations. The energy resolution for each point is found by combining the energy spread determined from scanning a finite length of plate and the loss of energy by ionization in traversing the thickness of target.

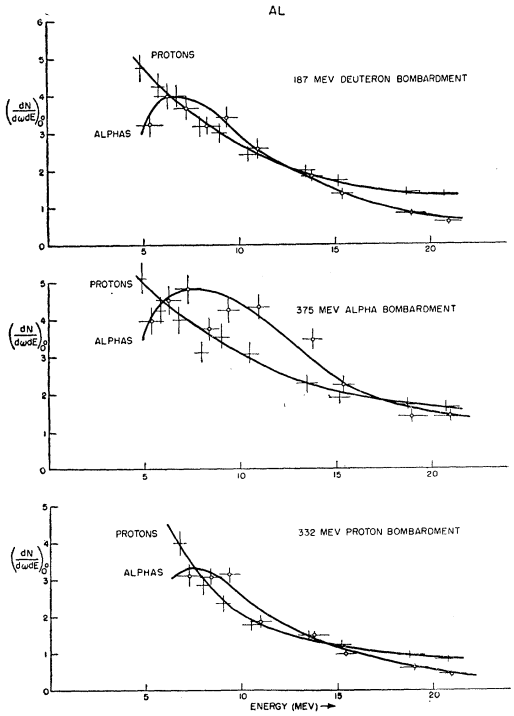

FIG. 6. Yields of secondary protons and alphas emitted at 0° to the incident beam direction as a function of their energy. (See caption to Fig. 5.)

the apparatus shown in Fig. 1. However, for the angular distribution, Fig. 2, the Jacobian is the same for each position, as ρ_H and h are the same in each position.

Finally, expression (4) is transformed into a function of the energy by using a nonrelativistic relationship between energy and momentum such that:

$$\frac{\Delta N}{\Delta E \Delta \omega} = \frac{\rho}{2E} \frac{\Delta N}{\Delta \rho \Delta \omega}. \tag{5}$$

IV. EXPERIMENTAL RESULTS

A. Momentum Distribution at 0°

Table II gives the abundance distribution of secondary particles obtained for 375-Mev alpha bombard-

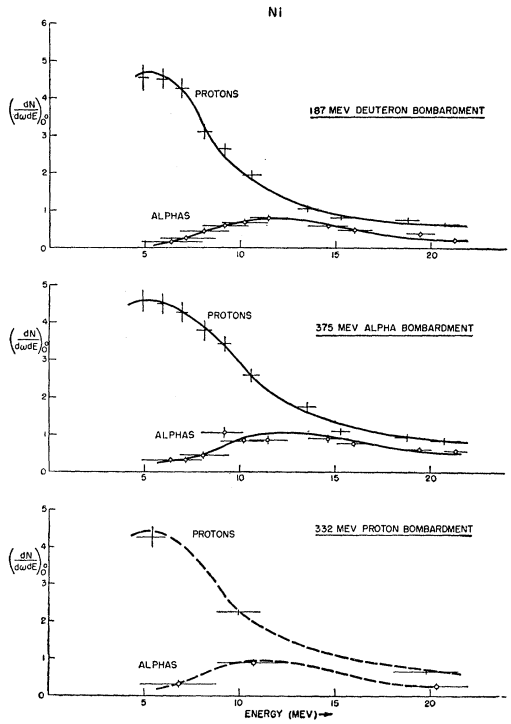

FIG. 7. Yields of secondary protons and alphas emitted at 0° to the incident beam direction as a function of their energy. (See caption to Fig. 5.)

ment. Tables III and IV give similar results found for 332-Mev proton and 187-Mev deuteron bombardments. In these tables, each element has been normalized to 100 percent for the number of particles found per unit solid angle per unit radius-of-curvature interval. The numbers not in parentheses are the percent values of each secondary particle found. The figures in parentheses are the actual numbers of tracks found. The method for reducing the data to this form has been described in the previous section.

The spectra of the protons and alphas that were obtained with the modified apparatus are shown in Figs. 5–10 for each bombardment. These figures give

the yields of protons and alphas relative to each other expressed in arbitrary units. The points are connected by a smooth curve drawn in an arbitrary fashion. It is not possible to compare different bombardments of the same element directly as such a comparison would require measurement of the absolute yields. Lack of time did not permit the scanning of the plates for the proton bombardment of Ni, Au, and U. For these bombardments, the results as listed in Table III are given with the expected curves. In all these plots, the errors shown for the number of particles found are statistical errors expressed in standard deviations. The

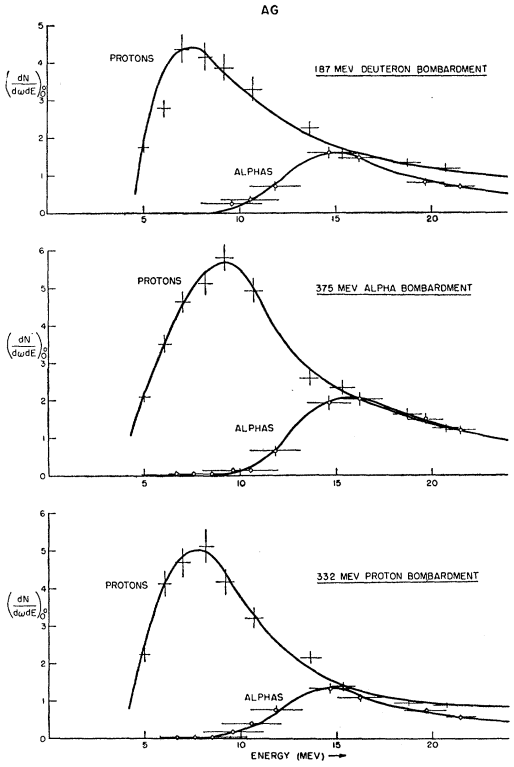

FIG. 8. Yields of secondary protons and alphas emitted at 0° to the incident beam direction as a function of their energy. (See caption to Fig. 5.)

energy resolution for each element shown is found by combining the finite length of plate with the loss of energy by ionization caused by the finite thickness of the target. The ionization loss for protons and alphas in Be, Al, and Ag targets was found directly from Aron's range-energy curves.[29] The ionization loss in the Ni, Au, and U targets was found by extrapolating the results for Cu and Pb, respectively, considering the change in electron density.

[29] Aron, Hoffman, and Williams, University of California Radiation Laboratory Report UCRL-121, AECU-663, 1949 (unpublished).

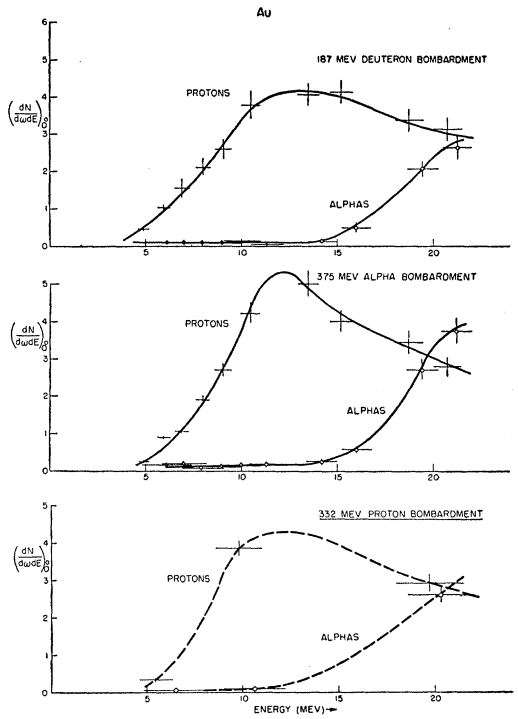

FIG. 9. Yields of secondary protons and alphas emitted at 0° to the incident beam direction as a function of their energy. (See caption to Fig. 5.)

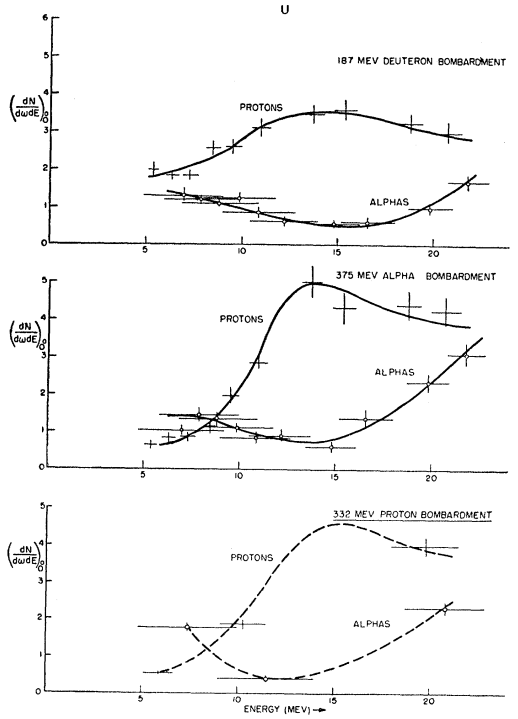

FIG. 10. Yields of secondary protons and alphas emitted at 0° to the incident beam direction as a function of their energy. (See caption to Fig. 5.)

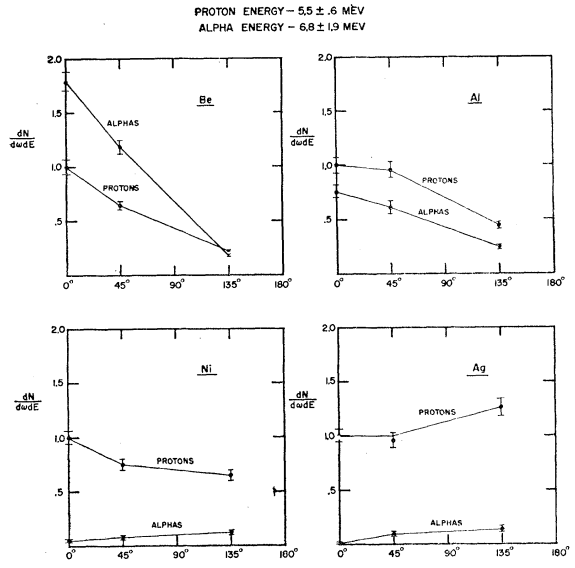

FIG. 11. Relative yields for the angular distribution of secondary protons and alphas resulting from 240-Mev alpha bombardment of Be, Al, Ni, and Ag. The number of tracks found per unit solid angle per unit energy interval is in arbitrary units.

B. Angular Distribution

Tables V to VII give the results obtained for Be, Al, Ni, and Ag for 240-Mev alpha bombardment. In these tables, each element has been normalized to 100 percent for the number of particles found per unit solid angle per unit radius-of-curvature interval. The numbers not in brackets are the percent values for each secondary particle found. The numbers in brackets are the actual numbers of tracks found. Figure 11 is a plot of the relative yields of protons and alpha particles (the errors shown are statistical errors). The energies of the protons considered are 5.5±0.6 Mev, while the energies of the alpha particles are 6.8±1.9 Mev.

The results for Au and U have not been included. The results for different exposures for these elements were inconsistent and not very reproducible. However, the yields from these bombardments were quite low, the flux of secondary particles being less than one hundredth as much, for the same bombarding time, as for the other elements. The fact that the yields are low for Au and U is not surprising, since the energies of the secondary particles are well below the Coulomb barrier for these elements. For extremely low yields, it is to be expected that any background effects, such as stray particles striking the cart and shielding and being scattered into the plates or producing secondary particles which enter the plates and satisfy the angular and range criteria, will be greatly magnified. All the elements with the exception of Be were run more than once, and there was always agreement well within statistics for the different exposures of the same element except in the case of Au and U. The results given in Fig. 11 for Be, Al, Ni, and Ag show that the angular distributions of the protons and alphas change very definitely as a function of atomic number, indicating that the background effects are small for these cases.

The failure to measure the angular distribution of Au and U for these low-energy secondary particles should not cast doubt on the results obtained for Au and U by using the apparatus which measured the momentum distribution at 0°. Here the results of different exposures for the same bombarding particles were reproducible, although the low-energy alpha yield fluctuated for reasons explained in Sec. V-B. The angular distribution apparatus is known to have a higher background; only alpha bombardment of the targets is possible. The higher background in the angular distribution apparatus is due to several factors. The plates have less shielding around them; the median plane of the cyclotron is one inch or 50 percent closer to the top of the cart at the target position, and the plates are set higher in the cart and therefore are closer to the median plane.

TABLE V. Relative abundances of products emitted at 0°, 45°, and 135° to the incident beam direction for 240-Mev alpha bombardment. Each element has been normalized to 100 percent for the number of particles found per unit solid angle per unit radius-of-curvature interval. The actual number of tracks found is in parentheses listed below the percentage in each case.

Bombarded element Angular position	Be 0° position	Be 45° position	Be 135° position
H^1	13.67	8.80	2.95
	(210)	(252)	(324)
H^2	4.30	2.27	0.77
	(66)	(65)	(83)
H^3	2.61	2.41	0.57
	(40)	(69)	(63)
He^3	4.43	2.55	0.62
	(68)	(73)	(68)
He^4	24.42	16.14	2.49
	(375)	(462)	(273)
Li^6, Be^7	2.67	2.65	0.21
	(41)	(76)	(23)
Li^8	0.13	0.10	
	(2)	(3)	
Not classified	2.67	2.51	0.04
	(41)	(72)	(4)

V. DISCUSSION OF RESULTS

A. Angular Distribution of Protons and Alpha Particles

The most direct way of discerning the region of validity of the cascade and evaporation models is to measure the angular distribution of heavy nuclei for energies of the secondary particles varying from about 5 to 50 Mev. Because of the limitations of the size of the cart, the highest energy that could be measured for secondary protons and alphas in this experiment was approximately 6 Mev.

The results for Be and Al represented in Fig. 11 show a sharp falling off as a function of increasing angle. However, since alphas are the bombarding particles,

the center-of-mass velocity is undoubtedly high enough —even taking into account a considerable amount of incident momentum being carried off by fast ejected particles—that there will be a considerable difference between the distribution actually occurring in the center-of-mass system and that measured in the laboratory system. There has been no lower limit set as to the number of nucleons necessary for a statistical theory, such as the evaporation model, to be valid. Since the compound-nucleus theory holds for the lightest elements, it would not be too surprising if Be could be explained by a two-step process. Nevertheless, to disentangle the results enough to determine the center-of-mass distribution for these light elements requires a considerable amount of supposition concerning the nature of the process giving rise to the secondary particles, and such an analysis has not been attempted.

The results for Ni and Ag are shown in Fig. 11. For

TABLE VI. Relative abundances of products emitted at 0°, 45°, and 135° to the incident beam direction for 240-Mev alpha bombardment. Each element has been normalized to 100 percent for the number of particles found per unit solid angle per unit radius-of-curvature interval. The actual number of tracks found is in parentheses listed below the percentage in each case.

Bombarded element / Angular position	Al 0° position	Al 45° position	Al 135° position
H^1	20.65	19.75	9.18
	(198)	(194)	(229)
H^2	0.66	1.04	0.62
	(7)	(8)	(14)
H^3	0.63	1.31	0.44
	(6)	(13)	(11)
He^3	0.53	0.69	0.44
	(5)	(7)	(11)
He^4	15.77	12.58	4.97
	(152)	(122)	(127)
Li^6, Be^7	0.59	2.05	0.11
	(6)	(19)	(3)
Not classified	5.38	2.51	0.11
	(51)	(28)	(3)

these elements the center-of-mass velocity is small. For low-energy particles, however, it is significant, since in the region around 6 Mev the yield of protons is energy-dependent (as one can see from the results for Ni and Ag in Figs. 7 and 8). Thus, if the residual nucleus retains a major portion of the incident momentum, then for a constant laboratory energy, a proton emitted in the backward direction has ~1 Mev greater energy than a forward emitted proton. In this energy region, the proton yield for Ni is a decreasing function of energy, while the proton yield for Ag is an increasing function of energy. Therefore, an isotropic emission in the center-of-mass system would show a peaking in the forward direction for Ni and a rise in the backward direction for Ag. This is what is observed in Fig. 11. The solid angle factor in going from the center-of-mass system to the laboratory system should also be taken into account, although it is quite small at low velocities.

TABLE VII. Relative abundances of products emitted at 0°, 45°, and 135° to the incident beam direction for 240-Mev alpha bombardment. Each element has been normalized to 100 percent for the number of particles found per unit solid angle per unit radius-of-curvature interval. The actual number of tracks found is in parentheses listed below the percentage in each case.

Bombarded element / Angular position	Ni 0° position	Ni 45° position	Ni 135° position
H^1	36.34	27.29	23.64
	(267)	(241)	(225)
H^2	0.27	0.33	0.31
	(2)	(3)	(3)
H^3	0.13	0.33	0.42
	(1)	(3)	(4)
He^3	0.27	0.33	0.31
	(2)	(3)	(3)
He^4	1.91	3.05	4.20
	(14)	(27)	(40)
Li^6, Be^7		0.33	
		(3)	
Li^8	0.13		
	(1)		
Not classified	0.27	0.11	
	(2)	(1)	

This factor tends to cause a peaking in the forward direction, and probably affects Ni more than Ag, since the center-of-mass velocity is probably less for Ag than for Ni. Therefore, it appears that the proton angular distribution is isotropic for both Ni and Ag. The rise in the alpha yield with increased laboratory angle for both these elements can also be explained by similar arguments based on the fact that yield of alpha particles should be increasing with energy in the region.

B. Energy Distribution of Protons and Alpha Particles Emitted at 0°

1. Ag (Fig. 8)

The element that can best be compared with theory is Ag, Fig. 8. The predicted proton distribution for the

TABLE VIII. Relative abundances of products emitted at 0°, 45°, and 135° to the incident beam direction for 240-Mev alpha bombardment. Each element has been normalized to 100 percent for the number of particles found per unit solid angle per unit radius-of-curvature interval. The actual number of tracks found is in parentheses listed below the percentage in each case.

Bombarded element / Angular position	Ag 0° position	Ag 45° position	Ag 135° position
H^1	27.90	26.88	35.09
	(259)	(217)	(236)
H^2	0.11	0.12	0.15
	(1)	(1)	(1)
H^3	0.22	0.37	0.15
	(2)	(3)	(1)
He^3	0.11	0.12	0.15
	(1)	(1)	(1)
He^4	0.32	2.73	3.86
	(3)	(22)	(26)
Li^6, Be^7	0.11	0.99	0.15
	(1)	(8)	(1)
Not classified	0.11	0.37	
	(1)	(3)	

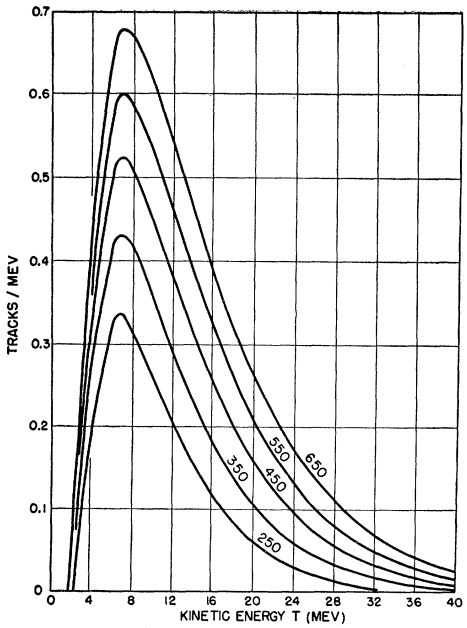

FIG. 12. The energy spectrum of the evaporated particles of charge e for five different values of the initial excitation energy. [LeCouteur (see reference 4)]

evaporation model as derived by LeCouteur is shown in Fig. 12. It can be seen that the shape of the curves is a very slowly varying function of excitation energy. The shapes of the experimentally determined proton spectra appear to be nearly similar for all bombardments. This fact is significant since, according to the evaporation model, the only effect of the bombarding particle should be in the total excitation energy given to the nucleus, and the resulting low-energy spectrum should be nearly independent of the primary process. In all cases, there is a maximum near 8 Mev. However, the position of the most probable energy appears to be increasing with excitation energy. That is, although the excitation energy is not known, the alpha bombardment should provide the highest excitation (believed to be $\sim$100 Mev) while the proton and deuteron bombardments probably have similar excitation energies (believed to be $\sim$50 Mev). This shift would be expected on a simple classical evaporation model, but LeCouter's curves indicate the most probable energy is independent of temperature. Also an evaporation model implies an exponential fall off in the yield for energies higher than the most probable energy, and the yield is definitely not falling off exponentially for the proton spectra. It appears, therefore, that a considerable number of these higher-energy protons originate from another process, probably the knock-out process postulated by Bernardini *et al.*

According to the evaporation model, the alpha particle distribution should have a peak at approximately twice the most probable proton energy. In all cases, this maximum is observed. However, here too the yield is not falling off exponentially for energies higher than the most probable alpha energy but indeed much less slowly. This discrepancy with the evaporation model implies that alpha particles are also knocked out of the nucleus. Bernardini *et al.* have not considered this possibility at all. As a matter of fact, they identify all their black tracks to be protons upon the assumption that the alpha particle emission is small compared to nucleon emission. However, for the proton bombardment which closely resembles the experiment of Bernardini *et al.*, the alpha-to-proton ratio is approximately 0.27 considering only energies of the secondary particles up to 24 Mev. Extrapolating to 30 Mev, the alpha-to-proton ratio is about 0.32. Thus, in terms of the black tracks of the Bernardini *et al.* experiment, about 25 percent of these black tracks are alpha particles.

2. *Ni* (*Fig. 7*)

The results for Ni are very similar to the Ag results. There appears to be a peak at about 5 Mev for the proton spectrum while the alpha spectrum has a maximum at about twice this value in agreement with an evaporation theory. However, here again the non-exponential fall-off in the yields for the high-energy protons and alphas are indicative of a knock-out process.

3. *Au and U* (*Figs. 9 and 10*)

For these elements, the evaporation model predicts that the probability of charged particle emission should be very small compared to neutron emission since the large Coulomb barrier for these elements prohibits charged particle emission. The proton spectra have very flat maxima in the vicinity of 13 Mev for Au and 15 Mev for U for all the bombardments, the shift in the peak with atomic number again being in accordance with an evaporation theory. However, the flatness of the maxima indicates the dominant form of emission for charged particles is the knock-out process for these elements.

The yield of alpha particles is rising at 20 Mev for both elements and not much can be said about the location of the maxima. The rise in the yield of alpha particles at low energies is attributed to slow alpha emitters created during the bombardment. Also, these slow alpha emitters undoubtedly cause fluctuations in the alpha yield, since the number of low-energy alphas detected is a function of the time the plates are left in the cyclotron after bombardment.

4. *Be and Al* (*Figs. 5 and 6*)

The Be bombardments are complicated by the center-of-mass velocity. Here as with the angular distribution, no attempt has been made to unravel these distributions to get the true emission spectra. Al, despite the comparatively few number of nucleons present, appears to have maxima in the regions that an evaporation model would predict.

C. Other Secondary Particles

Tables II–VIII indicate that an appreciable number of other particles are also emitted. However, the individual statistics as well as the energy resolution are quite poor for most of these particles. In comparison to the yields of protons and alphas, the yields of H^2, H^3 and He^3 particles are considerable only for the light elements, Be and Al. The depression of the yields of these particles for heavier elements is primarily a Coulomb barrier effect. In particular for the H^2 and H^3 particles, their energies are approximately $\frac{1}{2}$ and $\frac{1}{3}$ respectively of the proton energy so that only the lower part of the spectrum is measured which is the part that is suppressed by the Coulomb barrier.

The results also indicate that secondary particles, fragments of $A>4$, are also emitted with high momenta. The yields seem to follow the curve for binding energy per nucleon, being high for the light and heavy elements and having a minimum for Ni. Most of these heavy fragments from heavy nuclei undoubtedly result from the fission process. However, it is conceivable, in the light of the spectra of the secondary alphas, that some of them are produced by the knock-out process.

VI. GENERAL OBSERVATIONS

The results obtained in this experiment for the proton and alpha yields are consistent with the predictions of an evaporation model. The positions of the maxima for each element and the change of the maxima as a function of atomic number are in accordance with the theory. Also, for Ag, at energies at about 6 Mev the distributions of protons and alphas seem to be isotropic. On the other hand, the high-energy tail of the proton distribution found for Ag indicates a competitive knock-out process such as has been treated by a nucleon cascade theory. However, the high-energy tail found for the alpha spectra of Ag as well as the large abundance of those alpha particles ($\sim$25 percent of the black tracks) indicate a knock-out process for alpha particles which does not have a theoretical interpretation as yet.

VII. ACKNOWLEDGMENTS

I am indebted to Professor Walter H. Barkas for having suggested and guided this experiment and to Professor Robert L. Thornton for his continued interest in the experiment. I owe a huge debt of gratitude to Miss Esther Jacobson, whose speed, efficiency, and determination in scanning most of the plates permitted the compilation of so many data. My sincere thanks to Jimmy Vale and the 184-inch cyclotron crew for providing the necessary beams.

PHYSICAL REVIEW VOLUME 97, NUMBER 4 FEBRUARY 15, 1955

Nucleon Anomalous Moment in a Cut-Off Meson Theory*

M. H. FRIEDMAN†
Department of Physics, University of Illinois, Urbana, Illinois
(Received August 26, 1954)

The anomalous magnetic moments of the neutron and proton are calculated to fourth order by using a cut-off meson theory. The value obtained is 1.44 when one uses the same parameters as employed for fitting the meson-nucleon scattering data.

I. INTRODUCTION

A NUMBER of meson theory calculations have been carried out by using a cut-off model, the results of which seem to agree fairly well with experiment over the region of applicability. A summary of these results has been prepared.[1] This paper will deal with the calculation of the anomalous nucleon magnetic moments up to fourth order in the coupling constant. It will be seen that the f^4 corrections are small compared to the f^2 terms so that one has reason to believe that perturbation theory makes sense for this model. This point has been discussed in more complete detail for the general case.[2]

II. HAMILTONIAN

The Hamiltonian chosen corresponds to the derivative coupling of pseudoscalar mesons with a fixed extended source. The electromagnetic interactions do not include those involving the nucleon currents, which we assume to be small because of the elimination of high momentum mesons and hence large nucleon recoils.

The theory may be made gauge-invariant in an infinite number of ways. One such[3] is to modify the usual

* This work was supported in part by the Office of Naval Research.
† Now at Physics Department, Columbia University, New York, New York.
[1] G. F. Chew (to be published).
[2] G. F. Chew, Phys. Rev. 94, 1755 (1954).
[3] R. G. Sachs (private communication).